Automatica 123 (2021) 109293

Contents lists available at ScienceDirect

Automatica

journal homepage: www.elsevier.com/locate/automatica

Brief paper

A new control framework for flapping-wing vehicles based on 3D pendulum dynamics ☆

Nak-seung P. Hyun [a,*], Rebecca McGill [a], Robert J. Wood [a,b], Scott Kuindersma [a]

[a] John A. Paulson School of Engineering and Applied Sciences, Harvard University, Cambridge, MA 02138, USA
[b] Wyss Institute for Biologically Inspired Engineering, Harvard University, Cambridge, MA 02138, USA

ARTICLE INFO

Article history:
Received 23 January 2019
Received in revised form 30 May 2020
Accepted 8 September 2020
Available online 26 October 2020

Keywords:
Application of nonlinear analysis and design
Flapping-wing vehicle
Partial feedback linearization
Minimum phase
Adaptive control
Tracking
3D pendulum

ABSTRACT

In this paper, a new control framework for an insect-scale flapping-wing vehicle is presented that exploits passive aerodynamic effects to stabilize the attitude dynamics. Many flapping-wing robotic flyers and flying insects share a common morphological feature in that the center of mass (CoM) is below the center of pressure (CoP), which makes the hovering configuration intrinsically unstable with open-loop control. Motivated by the fact that the CoM should be ahead of the CoP to ensure the longitudinal stability of the flight dynamics, a new coordinate system is proposed by placing a virtual control point (VCP) above the CoP. The dynamics in the new coordinates are derived using a near-identity diffeomorphism which admits a partial feedback linearization with stable zero dynamics. The behavior of the zero dynamics resembles the dynamics of a 3D pendulum with an aerodynamic damper. An adaptive controller is proposed to make the upright orientation almost globally asymptotically stable over a bounded uncertainty of the aerodynamic drag coefficient. The controller is evaluated in simulation with a Harvard RoboBee following a virtual control point reference trajectory.

1. Introduction

Over recent decades, research in the field of small-scaled flapping-wing micro aerial vehicles (FWMAV) has rapidly expanded, inspired by the ability of flying insects to perform aggressive maneuvers with seemingly effortless ease. Analysis of the morphological parameters of various flying insects has shown that the wing base attached to the body is often higher than the insect's center of mass (CoM) (Ellington, 1984). This unique feature is reflected in many insect-scale FWMAV, including the Harvard RoboBee (81mg and 170 Hz flapping frequency) (Ma, Chirarattananon, Fuller, & Wood, 2013), the CMU piezoelectric-driven FWMAV (160mg and resonance at 35 Hz flapping frequency) (Hines, 2012), and the motor driven robotic Hummingbird prototype (12g and 34 Hz flapping frequency) described in Zhang, Fei, et al. (2017).

Past research suggests that the vertical displacement between the CoM and the wing base introduces a body pitch oscillation which renders hovering intrinsically unstable, resulting from the aerodynamic drag acting on each wing (Cheng & Deng, 2011; Ristroph et al., 2013; Teoh et al., 2012). The open-loop instability of hovering has been extensively studied in model-based simulations, which have demonstrated this effect using techniques including the application of differential geometric higher-order averaging (Taha, Woolsey, & Hajj, 2015), the use of Floquet theory to analyze hovering stability in periodic orbits (Su & Cesnik, 2011), and simplification via disregarding the wing inertial effects (Cheng & Deng, 2011; Ristroph et al., 2013; Teoh et al., 2012). See Taha, Hajj, and Nayfeh (2012) for surveys of control methods.

Prior work on hovering control for FWMAV has leveraged generalized averaging theory (Taha et al., 2015) and geometric methods similar to those used in standard quadrotor control (Ma et al., 2013; Zhang, Tu, et al., 2017). These controllers operate by suppressing the unstable part of the dynamics to locally stabilize while hovering. (An extensive review of the control architectures of FWMAV can be found in Taha et al., 2012.) In particular, previous controllers for the Harvard RoboBee have treated the instability resulting from the separation between the CoM and the center of pressure (CoP) (on average at the wing base of the vehicle, as in Fig. 1) as an attitude disturbance, rejecting it with other force and torque disturbances experienced in flight. Techniques used to stabilize vehicle pitch in this manner include the addition of a rotational damper to achieve passive

☆ The material in this paper was not presented at any conference. This paper was recommended for publication in revised form by Associate Editor Abdelhamid Tayebi under the direction of Editor Thomas Parisini.

* Corresponding author.
E-mail addresses: pathyun@gmail.com (N.-s.P. Hyun), rhsteinmeyer@seas.harvard.edu (R. McGill), rjwood@seas.harvard.edu (R.J. Wood), scottk@seas.harvard.edu (S. Kuindersma).

https://doi.org/10.1016/j.automatica.2020.109293
0005-1098/

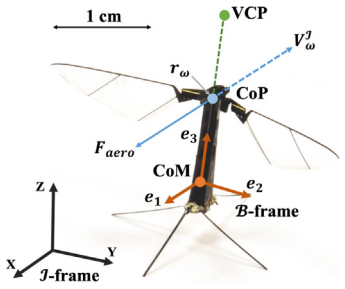

Fig. 1. Harvard RoboBee coordinates. (For interpretation of the references to color in this figure legend, the reader is referred to the web version of this article.)

attitude stability (Teoh et al., 2012), the application of a simple torque proportional to the angular velocity to stabilize the upright orientation (Fuller, Karpelson, Censi, Ma, & Wood, 2014), and the design of an adaptive sliding mode controller to reject unmodeled disturbances (including those due to CoM and CoP separation) (Chirarattananon et al., 2017).

Instead of rejecting the aerodynamic drag effects, we present a new approach designed to take advantage of the drag in order to stabilize the upright orientation of FWMAV. This idea is motivated by the principle that the CoM should lie above the CoP to obtain static stability in flight (Anderson, 2011). A controller is designed to stabilize a virtual control point (VCP) along the body z axis above the vehicle, as shown in Fig. 1. The system is then analogous to a 3D pendulum, where the VCP serves as the pivot point, and the stroke-averaged aerodynamic damping at the CoP dampens attitude oscillations (since the pivot point lies above the CoP). This is understood by considering the near-identity diffeomorphism introduced in Olfati-Saber (2002), which controls nonholonomic $SE(2)$ vehicles. Both the proposed near-identity diffeomorphism in this paper and that in Olfati-Saber (2002) allow partial feedback linearization with stable zero dynamics. However, the stability proof in Olfati-Saber (2002) cannot be directly transferred, as its asymptotic stability comes from a nonholonomic constraint and there are no such nonholonomic constraints for the dynamics considered herein. The proposed controller guarantees almost global asymptotic stability (AGAS) to the desired invariant set (the hovering configuration), similar to control of a 3D pendulum with a fixed base pivot (Chaturvedi, McClamroch, & Bernstein, 2009). Additionally, the VCP-based controller is advantageous in its reduced requirement for yaw torque during trajectory tracking, which is commonly a weak controlled torque for FWMAV (Calderón et al., 2019; Fei, Tu, Zhang, & Deng, 2019; Hines, Arabagi, & Sitti, 2011; Yang, Chen, Chang, Calderón, & Pérez-Arancibia, 2019) An adaptive controller is also proposed to show robustness over bounded uncertainty in the aerodynamic drag coefficient using the projection-based adaptation in Lavretsky and Gibson (2011). This proposed adaptive controller also preserves the AGAS property. Finally, an application is demonstrated in the design of a tracking controller, following a reference trajectory with the VCP in simulation.

2. Modeling

We consider a standard rigid body dynamics model (six degrees of freedom) with a stroke-averaged aerodynamic force, controlled via the thrust and torque acting on the rigid body. This model, and underlying assumptions, are appropriate for insect-scale FWMAVs due to their relatively small wing mass. We use the Harvard RoboBee as an example system for this work. The vehicle flies via amplitude-modulated harmonic voltage signals which each drive a piezoelectric bimorph actuator with a resonant frequency of approximately 170 Hz, and has a wing mass less than 1% of its the total body weight (Finio, Pérez-Arancibia, & Wood, 2011). Previous control approaches for this system (Chirarattananon, Ma, & Wood, 2016; Ma et al., 2013) have found desired thrust and torques, then converted these to voltage signals using a predefined mapping (Ma et al., 2013).

Let the $\mathcal{I}$-frame and $\mathcal{B}$-frame represent the inertial and body-fixed frames, respectively, as shown in Fig. 1. The origin of the $\mathcal{B}$-frame is located at the center of mass (CoM) position and its orientation aligns with the principal axis of the vehicle, such that its z-direction coincides with the direction of thrust. The configurations of a rigid body can be represented by the special Euclidean group, $SE(3)$, which is a semi-direct product of $\mathbb{R}^3$ and the special orthogonal group $SO(3)$. In this paper, (r, R) denotes a homogeneous coordinate (Murray, 2017) of $SE(3) \cong \mathbb{R}^3 \rtimes SO(3)$, in which r represents the origin of $\mathcal{B}$-frame in the $\mathcal{I}$-frame, and R represents the orientation of $\mathcal{B}$-frame relative to the $\mathcal{I}$-frame.

Let v be the velocity of the CoM in the $\mathcal{I}$-frame, $\omega \in \mathbb{R}^3$ be the instantaneous body angular velocity, m be the total mass, g be the gravity, and I be the moment of inertia. By using the conventional hat operation, $\widehat{\cdot}: \mathbb{R}^3 \to so(3)$, where $so(3) \subset \mathbb{R}^{3\times3}$ is the space of skew-symmetric matrices, the full rigid body dynamics are

$$\dot{r} = v \tag{1}$$
$$\dot{R} = R\widehat{\omega} \tag{2}$$
$$\dot{v} = -ge_3 + TRe_3 + F_{aero}/m \tag{3}$$
$$I\dot{\omega} = -\omega \times I\omega + \tau + \tau_{aero}, \tag{4}$$

where $\times$ is a cross product, $e_3 = (0, 0, 1)^\top$ is an elementary unit vector in $\mathbb{R}^3$, T is a thrust normalized by the mass, and $\tau = (\tau_1, \tau_2, \tau_3)$ is an external torque. The dynamics in (3)–(4) contain the aerodynamic drag force, F_{aero}, and the induced torque, τ_{aero}. The moment of inertia, $I \in \mathbb{R}^{3\times3}$, is a diagonal matrix with (I_{xx}, I_{yy}, I_{zz}) as its diagonal components and a skew symmetric matrix, $\widehat{\omega}$, is given by a relation, $\widehat{\omega}y = \omega \times y$, and $\bar{0} \in \mathbb{R}^3$ represents the zero vector.

2.1. Stroke-averaged aerodynamic damping model

Wind tunnel experiments (Teoh et al., 2012) have shown that the stroke-averaged aerodynamic drag is approximately a linear function of the velocity of the center of pressure point of the wing. Let $b_w > 0$ be the stroke-averaged aerodynamic drag coefficient. By assuming the symmetric configuration of both wings, the stroke-averaged aerodynamic drag model can be formulated as

$$F_{aero} = -b_w(v + R(\omega \times r_w)) \tag{5}$$
$$\tau_{aero} = r_\omega \times R^\top F_{aero}, \tag{6}$$

where $r_w := le_3$ is the centroid of the two wing CoPs in $\mathcal{B}$-frame, and l is the distance to the CoM. The centroid of the CoP is shown as a blue circle in Fig. 1, and the CoM is shown as a red circle in Fig. 1. The velocity of the CoP, $V_w^{\mathcal{I}}$, and F_{aero} are also shown in the figure. The exact scale can be found in Fuller et al. (2014).

3. Preliminary notions of set-stability

Let $D := TSE(3)$ be the domain of (1)–(4), with $TSE(3)$ the tangent bundle of $SE(3)$. Suppose that $R_1, R_2 \in SO(3)$, then

$$d_R(R_1, R_2) := \|I_{3\times3} - R_1^\top R_2\|_F, \tag{7}$$

where $\|\cdot\|_F$ is a Frobenius norm in $\mathbb{R}^{3\times3}$, is a metric on $SO(3)$. See Huynh (2009) for the topological equivalence between different metrics of $SO(3)$. Suppose that $x = (r_x, R_x, v_x, \omega_x) \in D$

and $y = (r_y, R_y, v_y, \omega_y) \in D$. Then, a distance between two configurations is given by

$$d(x,y) := [\ \|r_x - r_y\|_2^2 + \|v_x - v_y\|_2^2 + \|\omega_x - \omega_y\|_2^2 + d_R(R_x, R_y)^2]^{1/2}.$$

A distance to a set using the above metric is defined as

$$\|x\|_{\mathcal{M}} := inf_{y\in\mathcal{M}} d(x,y). \tag{8}$$

The following definition of set-stability is used in this paper. A similar definition can be found using the comparison functions in Lin, Sontag, and Wang (1996), and the "almost global" property can be found in Lee (2015).

Definition 1. A set $\mathcal{M} \subset D$ is

(1) stable with respect to (1)–(4), if for $\epsilon > 0$, there exists $\delta(\epsilon) > 0$ such that if $\|x(0)\|_{\mathcal{M}} < \delta(\epsilon)$, then $\|x(t)\|_{\mathcal{M}} < \epsilon$,
(2) attractive with respect to (1)–(4), if there exists an open neighborhood U of $\mathcal{M}$ such that if $x(0) \in U$, then $\lim_{t\to\infty} \|x(t)\|_{\mathcal{M}} = 0$.

The set is asymptotically stable if the set is both stable and attractive. In addition, the set is almost globally asymptotically stable if it is asymptotically stable and the set of initial conditions such that $\lim_{t\to\infty} \|x(t)\|_{\mathcal{M}} \neq 0$ has a zero Lebesgue measure.

4. A new coordinate system via near-identity diffeomorphism

In this section, a new coordinate for the dynamics in (1)–(4) is proposed by using a near-identity diffeomorphism. Pick a positive $\alpha \in \mathbb{R}^+$ and consider the following mapping, $\Phi_\alpha : D \to D$, defined everywhere in the domain,

$$\Phi_\alpha(x) := \begin{pmatrix} \eta_1(x) \\ \eta_2(x) \\ R \\ \omega \end{pmatrix} = \begin{pmatrix} r + \gamma R r_w \\ v + \gamma R(\omega \times r_w) \\ R \\ \omega \end{pmatrix} \tag{9}$$

where $\gamma = 1 + \alpha$. It is obvious that Φ_α is invertible, and the Jacobian of Φ_α has full rank for all x, and so Φ_α is a global diffeomorphism. If $\alpha = -1$, then Φ_α becomes the identity map; therefore, this is a near-identity diffeomorphism. In this paper, $\alpha > 0$ is assumed. The intuition of this mapping is such that the origin of the body frame is shifted up by $(1+\alpha)Rr_w$, which is the direction of the body z axis. This new virtual control point (VCP) refers to the point above the CoP of the vehicle, shown by the green circle in Fig. 1.

Suppose that the vector field of (1)–(4) is rearranged to a control affine form with $(f(x), g(x))$ with drift $f(x)$, actuation $g(x)$, and control $u = (T, \tau)$. Observe that $\dot\eta_1(x) = \eta_2(x)$, and by defining $\eta_1(x)$ as an output of the system, the dynamics of the new coordinate in (9) can be transformed to an almost normal form (the control term appears in the zero dynamics). The Lie derivatives of η_1 along with f and g (see definitions in Khalil, 2002) are

$$L_f^2\eta_1(x) = f_1(R,\omega) - b_w(C_1(R)\eta_2(x) + C_2(R)\omega) \tag{10}$$

$$L_gL_f\eta_1(x) = \left(Re_3; -\gamma R\widehat{r}_w I^{-1}\right), \tag{11}$$

where; indicates a column-wise concatenation, and

$$f_1(R,\omega) = -ge_3 + \gamma R\widehat{\omega}^2 r_w + \gamma R\widehat{r}_w I^{-1}(\widehat{\omega}I\omega)$$
$$C_1(R) = (\frac{1}{m}I_{3\times3} - \gamma R\widehat{r}_w I^{-1}\widehat{r}_w R^\top)$$
$$C_2(R) = \alpha R\widehat{r}_w(\frac{1}{m}I_{3\times3} - \gamma I^{-1}\widehat{r}_w^2).$$

Let $I_{3\times3}$ and $0_{3\times3}$ be the identity and zero matrices, and

$$A_c = \begin{pmatrix} 0_{3\times3} & I_{3\times3} \\ 0_{3\times3} & 0_{3\times3} \end{pmatrix}, B_c = \begin{pmatrix} 0_{3\times3} \\ I_{3\times3} \end{pmatrix}, E = \left(\bar{0}, I_{3\times3}\right).$$

The topologically conjugate system to (1)–(4) is derived,

$$\dot\eta = A_c\eta + B_c(L_f^2\eta_1 + A(R)u) \tag{12}$$
$$\dot R = R\widehat{\omega} \tag{13}$$
$$I\dot\omega = -\widehat{\omega}I\omega - b_w\widehat{r}_w R^\top(\eta_2 - \alpha R(\widehat{\omega}r_w)) + Eu, \tag{14}$$

where $\eta = (\eta_1, \eta_2)^\top$ and $A(R) := L_gL_f\eta_1(x)$. Observe that $L_gL_f\eta_1(x) \in \mathbb{R}^{3\times4}$, while not square, is full row rank, since $rank(\widehat{e}_3) = 2$, and $e_3^\top\widehat{e}_3 = \bar{0}$. This differs from a typical partial output feedback linearization since the system is not square; however, the row space of $L_gL_f\eta_1(x)$ is orthogonal to $e_4 := (0,0,0,1)^\top$, which indicates that $A(R)u$ in (12) is independent of the yaw torque τ_3. Therefore, the output dynamics can be fully controllable without a yaw torque input and the output dynamics can be feedback linearizable with three inputs, (T, τ_1, τ_2). In addition, the ω_3 state in $\Phi(x)$ is fully controllable with τ_3 and is independent of the output dynamics.

5. Stability analysis of partial feedback linearization controller

First, a partial feedback linearization controller is designed to exponentially stabilize the output to become zero, $\eta = \bar{0}$. Since $A(R)$ is full row rank, there exists a pseudo inverse, such that $A^\dagger(R) := A(R)^\top(A(R)A(R)^\top)^{-1}$.

5.1. Partial feedback linearization controller

We choose $Q_c \in \mathbb{R}^{6\times6}$ and $R_c \in \mathbb{R}^{3\times3}$ to be positive definite matrices and pick $k_w > 0$. Since (A_c, B_c) is controllable, there exists a unique positive definite $P \in \mathbb{R}^{6\times6}$ that solves the continuous-time algebraic Riccati equation (CARE) using (A_c, B_c, Q_c, R_c). The linear quadratic regulator (LQR) is then used to stabilize the output dynamics with gain $K := R_c^{-1}B_c^\top P$. Then, the state feedback controller can be defined as

$$u := A^\dagger(R)(-L_f^2\eta_1(x) - K\eta(x)) - k_w e_4\omega_3. \tag{15}$$

Note that a simple yaw control law, $\tau_3 = -k_w\omega_3$, in the last term is used but does not appear in the output dynamics in (12) since $A(R)e_4 = \bar{0}$ holds. Now, by substituting u in (12)–(14) with the controller in (15),

$$\dot\eta = (A_c - B_cK)\eta \tag{16}$$
$$\dot R = R\widehat{\omega} \tag{17}$$
$$\dot\omega = h(R,\omega) + g_1(R)\eta, \tag{18}$$

where $h(R,\omega) \in \mathbb{R}^{3\times1}$ and $g_1(R) \in \mathbb{R}^{3\times6}$ are

$$h(R,\omega) = \begin{pmatrix} \omega_2\omega_3 \\ -\omega_1\omega_3 \\ a_1(\omega_1\omega_2) - k_w\omega_3 \end{pmatrix} + \frac{b_w\alpha}{\gamma}(\widehat{e}_3^2\omega) + \frac{g}{l\gamma}(\widehat{e}_3R^\top e_3) \tag{19}$$

$$g_1(R) = \frac{1}{l\gamma}(\widehat{e}_3R^\top(\frac{b_w}{m}B_c^\top - K)) \tag{20}$$

and $a_1 = (I_{xx} - I_{yy})/I_{zz}$. If $I_{xx} = I_{yy}$, then the zero dynamics (when $\eta_1 = \eta_2 = \bar{0}$) equate to a 3D pendulum in Shen, Sanyal, Chaturvedi, Bernstein, and McClamroch (2004) with a rotational damping effect. By using the proposed controller, the aerodynamic drag acting on the CoP is transformed such that it behaves as a rotational damper in the new coordinate system, to eventually help stabilize to the upright orientation.

5.2. Set of equilibrium points

There exist two disjoint sets of equilibrium points for the nonlinear system in (16)–(18),

$$M_{up}^f := \{x \in D | \eta_1 = \eta_2 = \omega = \overline{0}, e_3^\top R^\top e_3 = 1\} \tag{21}$$

$$M_{inv}^f := \{x \in D | \eta_1 = \eta_2 = \omega = \overline{0}, e_3^\top R^\top e_3 = -1\}. \tag{22}$$

Geometrically, the condition for M_{up}^f represents the upright orientation with a free yaw angle, whereas the condition for M_{inv}^f represents the inverted orientation. This is akin to the hanging equilibrium and the inverted equilibrium for a 3D pendulum in Shen et al. (2004). The set of the union of two equilibrium sets is denoted as $M_{eq}^f = M_{up}^f \cup M_{inv}^f$.

5.3. Stability analysis of the full dynamics

In this section, the set-stability of two disjoint equilibrium sets is considered. Let the following function $V : D \to \mathbb{R}$ be defined as

$$V(x) := \nu^\top P_v \nu + \frac{g}{l\gamma}(1 - e_3^\top R e_3), \tag{23}$$

where $\nu \in \mathbb{R}^9$ and $P_v \in \mathbb{R}^{9\times 9}$ are defined as

$$\nu = \begin{pmatrix} R(e_3 \times \omega) \\ \eta \end{pmatrix}, \quad P_v = \begin{pmatrix} \frac{1}{2} I_{3\times 3} & 0_{3\times 6} \\ 0_{6\times 3} & k_p P \end{pmatrix}, \tag{24}$$

where $x = (\eta, R, \omega)$, $k_p > 0$, and $0_{3\times 6}, 0_{6\times 3}$ are zero matrices. Observe that V is only positive semi-definite since ω_3 does not appear in V. By taking the derivative of V along (16)–(18),

$$\dot{V}(x) = -\nu^\top P_f \nu, \tag{25}$$

holds for all $\nu \in \mathbb{R}^9$ and $P_f \in \mathbb{R}^{9\times 9}$ is defined as

$$P_f = \begin{pmatrix} \frac{b_w \alpha}{m\gamma} I_{3\times 3} & \frac{1}{2l\gamma}(\frac{b_w}{m} B_c^\top - K) \\ \frac{1}{2l\gamma}(\frac{b_w}{m} B_c^\top - K)^\top & k_p Q_c \end{pmatrix}. \tag{26}$$

Observe that P_f is a constant matrix, and it is a function of k_p. Let $S \in \mathbb{R}^{6\times 6}$ be a positive semi-definite matrix:

$$S := \frac{m}{4 b_w l^2 \gamma \alpha}(\frac{b_w}{m} B_c^\top - K)^\top (\frac{b_w}{m} B_c^\top - K). \tag{27}$$

Lemma 2. *If $k_p > \lambda_M(S)/\lambda_m(Q_c)$, where $\lambda_M(S)$ is the maximum eigenvalue of S and $\lambda_m(Q_c)$ is the minimum eigenvalue of Q_c, then P_f is positive definite.*

Proof. Since diagonal blocks of P_f are invertible, P_f is positive definite if and only if $k_p Q_c - S$ is positive definite by Theorem 7.76 in Horn and Johnson (1990). The condition for k_p suffices to show that $k_p Q_c - S$ is positive definite. □

5.3.1. Boundedness of the trajectories

Now, pick k_p to satisfy Lemma 2, then (25) implies that $\dot{V}(x) \leq 0$ for all $x \in D$. However, the sub-level set of V in (23) is unbounded as V is independent of ω_3. Therefore, the boundedness of the trajectories needs to be first shown before possibly applying LaSalle's invariance theorem (or Barbalat's lemma) for proving the attractiveness to the desired set. By considering the dynamics of yaw in (18) separately, the following proposition and corollary show that the trajectories of (16)–(18) are bounded for each initial condition.

Proposition 3. *There exists a class $\mathcal{K}$ function, $\beta_1 : [0, \infty) \to [0, \infty)$ such that, for any $\epsilon > 0$, if $|\omega_3(0)| < \epsilon$, then $\|\omega(t)\|_2 < \beta_1(\epsilon)$ for all $t \geq 0$.*

Proof. Suppose that $|w_3(0)| < \epsilon$, and pick $c_1 > 0$ such that $V(x(0)) \leq c_1\epsilon^2$, then $|\omega_1(t)\omega_2(t)| \leq 1/2(\omega_1^2(t) + \omega_2(t)^2) \leq c_1\epsilon^2$ holds for all $t \geq 0$ since $\dot{V}(x(t)) \leq 0$. By solving for $\omega_3(t)$ in (18), $|\omega_3(t)| \leq \epsilon + a_1 c_1 \epsilon^2/k_w$ holds. Also, by using the inequality for the l_1 and l_2 norms,

$$\|\omega(t)\|_2 \leq \|\omega(t)\|_1 \leq (2\sqrt{2c_1} + 1)\epsilon + a_1 c_1 \epsilon^2/k_w. \tag{28}$$

This is true for all $t > 0$. The right hand side of (28) can be shown to be a class $\mathcal{K}$ function over ϵ, hence the proposition holds. □

Corollary 4. *For any bounded open neighborhood, U, of M_{eq}^f, there exists a compact subset Ω_c such that if $x(0) \in U$, then $x(t) \in \Omega_c$ for all $t > 0$.*

Proof. Let $\Omega \in D$ be a closure of U. Since V is continuous, Ω is compact, and $\dot{V}(x(t)) \leq 0$, there exists $V_{max} > 0$ such that $V(\phi(x(t), y)) \leq V_{max}$ for every $y \in \Omega$ where $\phi(x(t), y)$ is a flow starting from y. Now, pick $\epsilon > 0$ such that all $x(0) \in \Omega$ satisfies $|\omega_3(0)| < \epsilon$, then by invoking Proposition 3, $\|\eta(t)\|_2^2 + \|\omega(t)\|_2^2$ is uniformly bounded for all $t \geq 0$ over every $x(0) \in U$. Hence, there exists a compact subset Ω_c such that $x(t) \in \Omega_c$ for all $t > 0$ since $SO(3)$ is compact.

5.3.2. Almost global asymptotic stability of M_{up}^f.

Next, the stability of M_{up}^f is shown as follows:

Theorem 5. *M_{up}^f is a stable set with respect to (16)–(18).*

Proof. Let $c_2 = max(\lambda_M(P_v), g/(l\gamma))$ and $\overline{\epsilon} < min(1, \lambda_m(P)/c_2)/\sqrt{10}$. Pick $\epsilon > 0$ such that $\epsilon < \overline{\epsilon}$. Suppose that the initial condition satisfies $\|x(0)\|_{M_{up}^f}^2 < \epsilon$, then $V(x(0)) \leq c_2\epsilon$ holds since

$$1 - e_3^\top R^\top e_3 \leq inf_{\psi\in[-\pi,\pi]} tr(I_3 - R^\top R_\psi)$$

holds for all $R \in SO(3)$ and all $e_3^\top R_\psi e_3 = \pm 1$. Since $\dot{V}(x) \leq 0$ for all $x \in D$, $\|\eta(t)\|_2^2 + \|\omega(t)\|_2^2 \leq c_2\epsilon/\lambda_m(P_v) + \beta_1(\sqrt{\epsilon})^2$ holds for all $t \geq 0$, where β_1 is a class $\mathcal{K}$ function proposed in Proposition 3.

The last step is to make sure the distance from $R(t)$ to the orientations of M_{up}^f (any $R_e \in SO(3)$ satisfying $e_3^\top R_e^\top e_3 = 1$) is bounded by some class $\mathcal{K}$ function over ϵ for all $t \geq 0$. Since R_e is a special orthogonal matrix, R_e can be represented by one parameter set $\psi \in [-\pi, \pi]$, where $e_1^\top R_\psi = [\cos\psi, -\sin\psi, 0]$, $e_2^\top R_\psi = [\sin\psi, \cos\psi, 0]$ and $e_3^\top R_\psi = e_3^\top$. Let (a_1, a_2, a_3) and (b_1, b_2, b_3) denote the first and second columns of $R^\top$, respectively. Observe that the Frobenius norm of the matrix can be represented by the trace operator, (Huynh, 2009), and that

$$inf_{\psi\in[-\pi,\pi]} d_R(R, R_\psi) = 3 - r - e_3^\top R^\top e_3$$

where $r = \sqrt{(a_1 + b_2)^2 + (a_2 - b_1)^2}$. Since R is in special orthogonal group, $det(R) = 1$, and $1 - e_3^\top R^\top e_3 < c_2\epsilon/\lambda_m(P_v)$, r is lower bounded by $r > \sqrt{4 - 40(c_2\epsilon/\lambda_m(P_v))^2}$. The lower-bound is well defined since $\epsilon < \overline{\epsilon}$ by the assumption. By substituting the lower-bound for r, $inf_{\psi\in[-\pi,\pi]} d_R(R, R_\psi) \leq \beta_4(\epsilon)$ holds where $\beta_4(\epsilon)$ is a class $\mathcal{K}$ function defined as $2 - \sqrt{4 - 40(c_2\epsilon/\lambda_m(P_v))^2} + \epsilon$. Hence, $\|x(t)\|_{M_{up}^f}^2 \leq c_2\lambda_m(P_v)\epsilon + \beta_1(\sqrt{\epsilon})^2 + \beta_4(\epsilon)$ for all $t \geq 0$, and so M_{up}^f is a stable set. □

Attractiveness to the set of equilibrium, M_{eq}^f, the union of M_{up}^f and M_{inv}^f, is shown in the following proposition.

Proposition 6. *M_{eq}^f is an attractive set with respect to (16)–(18).*

Proof. Let U be a bounded open neighborhood of M^f_{eq} such that $x(0) \in U$, and $g : [0, \infty) \to [0, \infty)$ be a twice differentiable function defined by $g(t) := V(x(t))$ using V in (23). Since $g(t)$ is lower bounded and $\dot{g}(t) \leq 0$ for all $t \geq 0$ by (25), $\lim_{t\to\infty} \int_0^t \dot{g}(t)dt$ exists and is finite. The second derivative of g, is expressed as $\ddot{g} = -2\nu P_f \dot{\nu}$, where $\nu := (\nu_1, \nu_2)$ such that $\nu_1 := R(e_3 \times \omega)$ and $\nu_2 := \eta$ as given in (24). Observe that $\dot{\nu}_1 = R\hat{\omega}(e_3 \times \omega) + R(e_3 \times \dot{\omega})$, and $\dot{\nu}_2 = \dot{\eta}$, where $\dot{\eta}$ and $\dot{\omega}$ are given in (16)–(18). Since the trajectory is bounded in some compact set, Ω_c, as shown in Corollary 4, $\ddot{g}(t)$ is also bounded for all $t \geq 0$. Therefore, $\dot{g}$ is uniformly continuous, and by invoking Barbalat's lemma (Khalil, 2002), $\lim_{t\to\infty} \dot{g} = 0$ holds. Since P_f in (26) is chosen to be positive definite by satisfying Lemma 2, $\lim_{t\to\infty} \|\nu(t)\| = 0$ holds, which infers that $\lim_{t\to\infty} \|\eta(t)\|_2 = 0$ and $\lim_{t\to\infty}(\omega_1^2 + \omega_2^2) = 0$.

In addition, $\lim_{t\to\infty} \|v\|_2 = 0$ also holds as $v = \eta_2 + l\gamma\nu_1$ is defined in (9). Let $g_i^v : [0, \infty) \to \mathbb{R}$ be defined as $g_i^v(t) := v_i(t)$ where v_i is i-th component of v, then $\lim_{t\to\infty} \int_0^t \dot{g}_i^v(t)dt$ exists and is finite where $\dot{g}_i = e_i^\top \dot{v}$. Also, $\ddot{g}_i(t)$ is bounded for all $t \geq 0$ since $\ddot{g}_i^v := e_i^\top \ddot{v}$, where $\ddot{v}(t) = \dot{\eta}_2 + l\gamma\dot{\nu}_1$, is a function of bounded quantities, according to Corollary 4. By invoking Barbalat's lemma, $\lim_{t\to\infty} \dot{g}_i^v(t) = 0$ holds, and so $\lim_{t\to\infty} \|\dot{v}(t)\|_2 = 0$ holds. Observe that

$$\lim_{t\to\infty}(-\gamma R\hat{e}_3^2 R^\top e_3) = \lim_{t\to\infty} \dot{v}(t) = 0$$

holds since $\lim_{t\to\infty} \|\eta\|_2 = 0$ and $\lim_{t\to\infty}(\omega_1^2 + \omega_2^2) = 0$. Therefore, $\lim_{t\to\infty} e_3 \times R^\top e_3 = 0$ holds, or equivalently, $\lim_{t\to\infty} e_3^\top R e_3 = 1$ or -1.

Now, pick $\epsilon < \bar{\epsilon}$ as in the proof of Theorem 5, then there exist $T_1 > 0$ such that if $t > T_1$, then $|\omega_1(t)\omega_2(t)| \leq \epsilon$ and $\|x(t)\|^2_{M^f_{eq}} \leq \epsilon + \omega_3(t)^2$ holds. By invoking the comparison lemma (Lemma 3.4 in Khalil, 2002) to the dynamics for ω_3 in (18), there exist $c_3 > 0$ and $T_2 > T_1$ such that if $t > T_2$, then $|\omega_3(t)| < c_3\epsilon$, and by invoking Proposition 3, $\|x(t)\|^2_{M^f_{eq}} < \epsilon + c_3^2\beta_1(\epsilon)^2$ for all $t > T_2$. Hence, $\lim_{t\to\infty} \|x(t)\|^2_{M^f_{eq}} = 0$ for all $x(0) \in U$. □

The first main theorem follows:

Theorem 7. *M^f_{up} is an almost globally asymptotically stable set with respect to (16)–(18).*

Proof. It is shown that M^f_{up} is locally stable in Theorem 5 and M^f_{eq} is globally attractive in Proposition 6. First the linearization around M^f_{inv} is considered. Pick $(\bar{0}, \bar{0}, R_{inv}, \bar{0}) \in M^f_{inv}$, and linearize (16)–(18) around this point. Observe that the linearized model for (R, ω) can be derived into a second order differential equation $(x_1, x_2, x_3) \in \mathbb{R}^3$,

$$\begin{pmatrix} \ddot{x}_1 \\ \ddot{x}_2 \\ \ddot{x}_3 \end{pmatrix} = \begin{pmatrix} -\frac{b_w\alpha}{\gamma}\dot{x}_1 + \frac{g}{l\gamma}x_1 \\ -\frac{b_w\alpha}{\gamma}\dot{x}_2 + \frac{g}{l\gamma}x_2 \\ 0 \end{pmatrix}. \tag{29}$$

This is similar to the linearization around an inverted equilibrium for a 3D pendulum in Chaturvedi, Lee, Leok, and McClamroch (2011) except that (29) has a damping term. There are two positive eigenvalues, two negative eigenvalues, and two zero eigenvalues. Since there are two positive eigenvalues, M^f_{inv} is an unstable set. Now, it is enough to show that the region of attraction for M^f_{inv} is a set of measure zero. The two zero eigenvalues correspond to the yaw rotation which is invariant in M^f_{inv}, and so the center manifold is contained in M^f_{inv}. Therefore, all the trajectories near $(\bar{0}, \bar{0}, R_{inv}, \bar{0})$ will diverge except the two-dimensional stable submanifold. This holds for any $(\bar{0}, \bar{0}, R_e, \bar{0}) \in M^f_{inv}$, so the stable submanifold has Lebesgue measure zero (Krstic & Deng, 1998). A similar argument can be found for the smooth control design in Chaturvedi et al. (2009). Hence, M^f_{up} is an AGAS set. □

6. Adaptive controller for a bounded uncertain drag coefficient

The AGAS property of the partial feedback linearizing controller was proven assuming perfect knowledge of the drag coefficient, which is not practically desirable. Nevertheless, it is interesting to observe that for any given $b_w > 0$, there exists at least one partial feedback linearizing controller to make the set, M^f_{up}, AGAS. By exploiting this fact, an adaptive controller is designed for a bounded uncertain drag coefficient. Assume that $b_w \in I_b$, where $I_b := [\underline{b}_w, \bar{b}_w]$, is bounded with $\underline{b}_w, \bar{b}_w > 0$. Now consider the following controller

$$u(x) := A^\dagger(R)(-L_f^2\eta_1(x, \widehat{b}_w) - K\eta(x)) - k_w e_4\omega_3 \tag{30}$$

$$\dot{\widehat{b}}_w := \begin{cases} 0 & \text{if } f_4(x) < 0 \text{ and } \widehat{b} = \underline{b}_w \\ 0 & \text{if } f_4(x) > 0 \text{ and } \widehat{b} = \bar{b}_w \\ \Gamma f_4(x) & \text{otherwise} \end{cases} \tag{31}$$

where $\Gamma > 0$ is the adaptation gain, and $L_f^2\eta_1(x, \widehat{b}_w)$ is the same as in (10), with $\widehat{b}_w$ instead of b_w,

$$f_4(x) := -2k_p^*\eta^\top PB_c(C_1(R)\eta_2/m + C_2(R)\omega) - \omega^\top I^{-1}\widehat{r}_w R^\top(\eta_2 - \alpha R(\widehat{\omega}r_w)),$$

and with initial condition, $\widehat{b}_w(0) \in I_b$.

Theorem 8. *M^f_{up} is an almost globally asymptotically stable set with respect to the closed loop dynamics with the adaptive controller in (30)–(31).*

Proof. Since the S matrix in (27) is a smooth function over b_w, there exists $\lambda_M^*(S) := max_{b_w\in I_b}\lambda_M(S(b_w))$. Now, pick $k_p^* > \lambda_M^*(S)/\lambda_m(Q)$; then, by Lemma 2, $P_f(\widehat{b}_w)$ from (26) is a positive definite matrix for any $\widehat{b}_w \in I_b$. Now, consider $V_1 : D \times I_b \to \mathbb{R}$ defined as $V_1(x, \widehat{b}_w) := V(x) + \Gamma^{-1}\widetilde{b}_w^2/2$ where $\widetilde{b}_w = b_w - \widehat{b}_w$ and $V(x)$ is (23). By taking the derivative,

$$\dot{V}_1 = -\nu^T P_f(\widehat{b}_w)\nu + f_4(x)\widetilde{b}_w + \Gamma^{-1}\widetilde{b}_w\dot{\widetilde{b}}_w \tag{32}$$

holds, and by substituting the adaptation law in (31), $\dot{V}_1(x, \widehat{b}_w) \leq -\nu^T P_f(\widehat{b}_w)\nu$ holds for all $x \in D$ as $f_4(x)\widetilde{b}_w \leq 0$ for $\widehat{b}_w = \underline{b}$ and $\widehat{b}_w = \bar{b}$. Observe that Proposition 3 and Corollary 4 still hold since $V(x) \leq V_1(x, \widehat{b}_w)$ and $\dot{V}(x(t)) \leq 0$ for all $t > 0$. Therefore, M^f_{up} is also a stable set, using the same argument as in Theorem 5.

Attractiveness to the equilibrium set, M^f_{eq}, is proven differently. Let $\lambda_m^*(P_f)$ be defined as $min_{\widehat{b}_w\in I_b}\lambda_m(P_f(\widehat{b}_w))$ where $\lambda_m(P)$ is the minimum eigenvalue of P, then $\|\nu(t)\|_2^2 \leq -\dot{V}_1/\lambda_m^*(P_f)$ holds for all $t \geq 0$. Therefore, ν is in the $\mathcal{L}^2$ space since

$$\int_0^\infty \nu(t)^\top\nu(t)dt \leq (V_1(0) - V_1(\infty))/\lambda_m^*(P_f)$$

where $V_1(\infty) := \lim_{t\to\infty} V_1(x(t), \widehat{b}_w(t))$, which is well defined as V_1 is lower bounded. In addition, $\|\nu(t)\|_2^2 < V_1(x(0), \widehat{b}_w(0))/\lambda_m^*(P_f)$ for all $t \geq 0$ indicates that ν is in the $\mathcal{L}^\infty$ space as well. Since $\widetilde{b}_w$ is bounded by the projection-based adaptive rule in (31), $\dot{\nu}(t)$ can be shown to be a bounded function as well. Therefore, $\lim_{t\to\infty} \|\nu\|_2 = 0$ by invoking the corollary of Barbalat's Lemma (Corollary 2.9 in Narendra & Annaswamy, 2012). Now the same argument of acquiring $\lim_{t\to\infty} \|\dot{\nu}(t)\|_2 = 0$ holds as $\widetilde{b}_w$ is bounded, which infers that $\lim_{t\to\infty} e_3^T R e_3 = 1$ or -1. Finally, considering the ultimate bound for $\omega_3(t)$ as in the proof of Proposition 6, M^f_{eq} can be shown to be asymptotically attractive.

Finally, the linearization around M^f_{inv} on each $\widehat{b}_w \in I_b$ exhibits two negative eigenvalues, indicating instability of M^f_{inv} with the Lebesgue measure zero stable sub-manifold, as in Theorem 7. Hence, M^f_{up} is an AGAS set. □

7. Application to VCP reference trajectory tracking

In this section, a direct application to the adaptive AGAS controller in (30) is considered to make the VCP follow a reference trajectory. Suppose that a continuously differentiable trajectory in the $\mathbb{R}^3$ space is given as $\phi \in C^2(\mathbb{R}, \mathbb{R}^3)$, where $C^2(\mathbb{R}, \mathbb{R}^3)$ is a set of continuously twice differentiable functions. Assume that the derivatives of the trajectory are bounded by some $M > 0$, such that $\|\dot{\phi}(t)\|_2 \leq M$ and $\|\ddot{\phi}(t)\|_2 \leq M$.

The objective is to make the VCP of the vehicle follow the reference trajectory. Defining error dynamics as $\xi_1 = \eta_1 - \phi$ and $\xi_2 = \eta_2 - \dot{\phi}$, and with $\xi = (\xi_1, \xi_2) \in \mathbb{R}^6$, then a feedback controller using ξ is proposed:

$$u := A^{\dagger}(R)(-L_f^2\eta_1(x, \widehat{b}_w) - K\xi(x) + \ddot{\phi}) - k_w e_4 \omega_3, \tag{33}$$

where $L_f^2\eta_1(x, \widehat{b}_w)$ is defined as in the controller in (30) and the adaptation rule in (31) is modified such that only η in $f_4(x)$ is replaced with ξ and not η_2.

For any given set point, $\phi_0 \in \mathbb{R}^3$, by setting $\phi(t) = \phi_0$, the error $\xi(t)$ almost globally exponentially converges to $\bar{0}$, and $\omega(t)$ almost globally asymptotically converges to $\bar{0}$ using the above controller.

7.1. VCP trajectory following

The VCP error dynamics for ξ using (33) are

$$\begin{aligned} \dot{\xi} &= (A_c - B_c K)\xi - \widetilde{b}_w B_c \epsilon(\xi, R, \omega) \\ \epsilon(\xi, R, \omega) &= (C_1(R)(\xi_2 + \dot{\phi}) + C_2(R)\omega). \end{aligned} \tag{34}$$

Suppose that the gain K is chosen by solving CARE of $(A_c + k_c I_{6\times 6}, B_c, Q_c, R_c)$ for $k_c > 0$, then all the real parts of the eigenvalues of $(A_c - B_c K)$ are upper bounded by $-k_c$. Let V_1 be defined as in Theorem 8 by replacing η with ξ, then the derivative is computed as

$$\dot{V}_1(x) \leq -c\|\nu\|_2^2 - k_c\lambda_m(P)\|\xi\|_2^2 - \frac{1}{ml\gamma}\left\langle \nu_1, \widehat{b}_w\dot{\phi} + m\ddot{\phi}\right\rangle,$$

where $c = \lambda_m^*(P_f)$, and $x \in (\xi, R, \omega)$, and $\nu = (\nu_1, \nu_2) \in \mathbb{R}^9$ is redefined with $\nu_1 = R(e_3 \times \omega)$ and $\nu_2 = \xi$. In addition, the upper bounds for $\dot{V}$ can be formulated as

$$\begin{aligned} \dot{V}_1(x) &\leq -(c + k_c\lambda_m(P))\|\xi\|_2^2 - \|\nu_1\|_2(c\|\nu_1\|_2 - \mu(M)) \\ &\leq -(c + k_c\lambda_m(P))\|\xi\|_2^2 \qquad \text{if } \|\nu\|_2^2 \geq \frac{2\mu(M)^2}{c^2}, \end{aligned}$$

where $\mu(M) = (\bar{b}_w + m)/(ml\gamma)M$. Applying the above inequalities, it can be shown that there exists $T > 0$ such that if $t > T$, then $\|\nu\|_2 < 2g/(l\gamma) + 2\lambda_M(P_v)\mu(M)^2/(c^2\lambda_m(P_v))$. Therefore, $\|\xi\|_2$ and $\|\omega\|_2$ are ultimately bounded.

The extra control gain, k_c, in addition to the LQR parameters, R_c and Q_c, is used to directly lower the real part of the eigenvalue of $(A_c - B_c K)$ in (34). In the ideal case (when $\widetilde{b}_w$ is zero or equivalently using the partial feedback linearization controller), the tracking error, $\|\xi\|_2$, converges exponentially to zero with a guaranteed decaying rate of $-k_c$. A case study with two different k_c gains shows that the parameter error becomes relatively small (within 0.02% of its true value, for both cases), and a faster convergence to the same error bound is achieved by higher k_c. The detailed analysis on the relation between parameter convergence and the tracking performance remains the subject of future work.

7.2. Simulation results

In this section, a tracking controller is applied to follow a Lissajous curve. The desired trajectory, $\phi(t) \in \mathbb{R}^3$, is

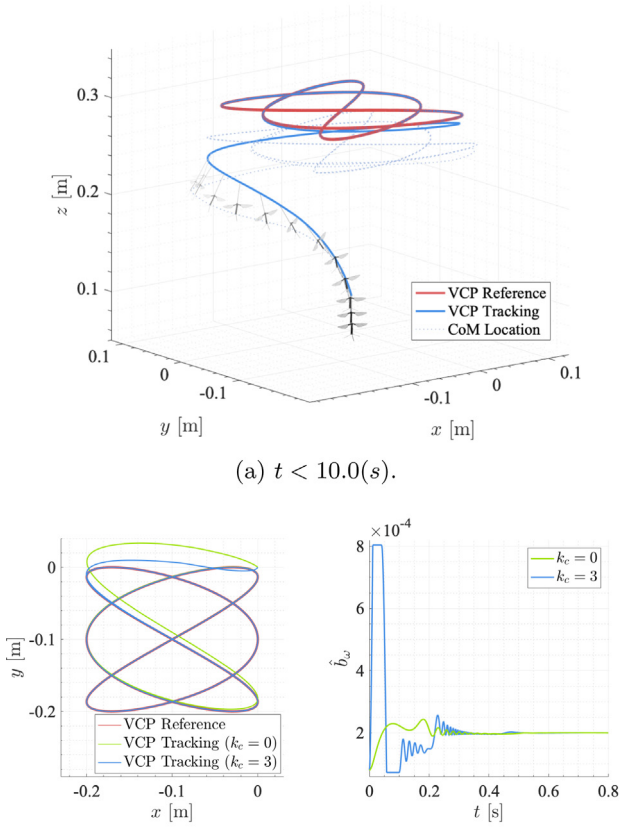

(a) $t < 10.0(s)$.

(b) VCP trajectory in (x, y). (c) Parameter estimation.

Fig. 2. Trajectories using different gains $k_c = 0, 5$. (For interpretation of the references to color in this figure legend, the reader is referred to the web version of this article.)

$$\phi_x(t) := r_d \cos(a\omega_f t + \delta) \tag{35}$$

$$\phi_y(t) := r_d \cos(b\omega_f t) \tag{36}$$

$$\phi_z(t) := 0.3, \tag{37}$$

where $r_d = 0.1, a = 2, b = 3$, and $\omega_f = 2\pi/T_{period}$, with $T_{period} = 1$ s. The model parameters for the Harvard RoboBee are given in Fuller et al. (2014), including $b_w = 2.0 \times 10^{-4}$ Ns m^{-1}. The bounds for the drag coefficients are given as $I_b = [0.4b_w, 4b_w]$ allowing higher upper bound. The tracking controller in (33) is applied, with the gain K designed using $Q_c = diag(100, 100, 100, 10, 10, 10)$ and $R_c = 0.01I_{3\times 3}$, with two different gains, $k_c = 0$ and $k_c = 3$. The adaptive gain is chosen with $\Gamma = 0.3$ for (31). A small feedback gain $k_w = I_{zz} = 0.45 \times 10^{-9}$ is chosen for yaw torque control. In this example, $\alpha = 3$ is selected (such that the VCP of the vehicle is four times higher than the CoP position). The chosen initial states are $r = (0, 0, 0.05)$, $v = \omega = \bar{0}$, and $R(0)$ is represented by the axis–angle representation, with angle $\theta_0 = \pi/4$ and axis $(1, 0, 0)$.

The simulation results are shown in Fig. 2(a). The trajectory of the VCP using the gain $k_c = 3$ is shown in blue, with the reference trajectory (a Lissajous curve at $z = 0.3$) shown in red. The CoM of the vehicle during VCP tracking is shown with a dotted blue line. Fig. 2(a) shows a forward simulation over 10.0 s (with overlaid orientations for the RoboBee shown over the first 0.5 s), demonstrating attitude changes as the VCP approaches the reference trajectory. A projection to the (x, y) plane is shown in Fig. 2(b), where the red curve represents the reference curve, the green curve corresponds to the VCP trajectory for $k_c = 0$, and the

blue curve corresponds to $k_c = 3$. The estimated drag coefficients are shown in Fig. 2(c) for both k_c gains. The parameter error is bounded to 0.02% of its true value after 0.5 s

8. Conclusions and discussion

In this paper, a new coordinate system for a flapping-wing vehicle is proposed, which takes advantage of the averaged aerodynamic drag acting on the vehicle. A state feedback controller is designed to regulate a virtual control point (VCP) using a near-identity diffeomorphism which permits partial feedback linearization. The stable zero dynamics resembles the 3D pendulum dynamics where VCP serve as a pivot. The almost global asymptotic stability of the upright configurations is shown for the closed loop system. Next, an adaptive controller is proposed, to preserve the AGAS property given the bounded uncertainty of the drag coefficient. Finally, a VCP tracking controller is designed to achieve ultimate boundedness.

One of the advantages of the VCP based control framework is that the controller requires relatively small yaw torque as the VCP output dynamics is independent of the yaw torque control. This is beneficial to FWMAV control as yaw torque is often a particularly weak torque axis for Calderón et al. (2019), Fei et al. (2019), Hines et al. (2011) and Yang et al. (2019). In addition, the proposed adaptation algorithm in (31) can be naturally combined with a deadzone method (Narendra & Annaswamy, 2012) to enhance the robustness to the bounded unmodeled disturbance.

Acknowledgments

The authors gratefully acknowledge support from the National Science Foundation, USA (Award No. IIS-1724197 and Graduate Research Fellowship Program, USA Grant No. DGE1745303), the Office of Naval Research, USA (Award No.N00014-17-1-2614), and the Wyss Institute for Biologically Inspired Engineering. Any opinions, findings, and conclusions or recommendations expressed in this material are those of the authors and do not necessarily reflect the views of the National Science Foundation.

References

Anderson, J. (2011). *Introduction to flight*. McGraw-Hill Education.

Calderón, A. A., Chen, Y., Yang, X., Chang, L., Nguyen, X. -T., Singer, E. K., et al. (2019). Control of flying robotic insects: A perspective and unifying approach. arXiv preprint arXiv:1910.11911.

Chaturvedi, Nalin A., Lee, Taeyoung, Leok, Melvin, & McClamroch, N. Harris (2011). Nonlinear dynamics of the 3D pendulum. *Journal of Nonlinear Science*, *21*(1), 3–32.

Chaturvedi, Nalin A., McClamroch, N. Harris, & Bernstein, Dennis S. (2009). Asymptotic smooth stabilization of the inverted 3-D pendulum. *IEEE Transactions on Automatic Control*, *54*(6), 1204–1215.

Cheng, Bo, & Deng, Xinyan (2011). Translational and rotational damping of flapping flight and its dynamics and stability at hovering. *IEEE Transactions on Robotics*, *27*(5), 849–864.

Chirarattananon, Pakpong, Chen, Yufeng, Helbling, E. Farrell, Ma, Kevin Y., Cheng, Richard, & Wood, Robert J. (2017). Dynamics and flight control of a flapping-wing robotic insect in the presence of wind gusts. *Interface Focus*, *7*(1), Article 20160080.

Chirarattananon, Pakpong, Ma, Kevin Y., & Wood, Robert J. (2016). Perching with a robotic insect using adaptive tracking control and iterative learning control. *International Journal of Robotics Research*, *35*(10), 1185–1206.

Ellington, Charles Porter (1984). The aerodynamics of hovering insect flight. II. Morphological parameters. *Philosophical Transactions of the Royal Society of London. Series B: Biological Sciences (London)*, *305*(1122), 17–40.

Fei, Fan, Tu, Zhan, Zhang, Jian, & Deng, Xinyan (2019). Learning extreme hummingbird maneuvers on flapping wing robots. In *Proc. international conference on robotics and automation* (pp. 109–115). IEEE.

Finio, Benjamin M., Pérez-Arancibia, Néstor O., & Wood, Robert J (2011). System identification and linear time-invariant modeling of an insect-sized flapping-wing micro air vehicle. In *Proc. international conference on intelligent robots and systems* (pp. 1107–1114). IEEE.

Fuller, Sawyer B., Karpelson, Michael, Censi, Andrea, Ma, Kevin Y., & Wood, Robert J. (2014). Controlling free flight of a robotic fly using an onboard vision sensor inspired by insect ocelli. *Journal of the Royal Society Interface*, *11*(97), Article 20140281.

Hines, Lindsey (2012). *Design and control of a flapping flight micro aerial vehicle*.

Hines, Lindsey L., Arabagi, Veaceslav, & Sitti, Metin (2011). Free flight simulations and pitch and roll control experiments of a sub-gram flapping-flight micro aerial vehicle. In *Proc. international conference on robotics and automation* (pp. 1–7). IEEE.

Horn, R. A., & Johnson, C. R. (1990). *Matrix analysis*. Cambridge University Press.

Huynh, Du Q. (2009). Metrics for 3D rotations: Comparison and analysis. *Journal of Mathematical Imaging and Vision*, *35*(2), 155–164.

Khalil, Hassan K. (2002). *Noninear systems. 3*. New Jersey: Prentice-Hall.

Krstic, M., & Deng, H. (1998). *Communications and control engineering, Stabilization of nonlinear uncertain systems*. Springer London.

Lavretsky, Eugene, & Gibson, Travis E. (2011). Projection operator in adaptive systems. arXiv preprint arXiv:1112.4232.

Lee, Taeyoung (2015). Global exponential attitude tracking controls on SO(3). *IEEE Transactions on Automatic Control*, *60*(10), 2837–2842.

Lin, Yuandan, Sontag, Eduardo D., & Wang, Yuan (1996). A smooth converse Lyapunov theorem for robust stability. *SIAM Journal on Control and Optimization*, *34*(1), 124–160.

Ma, Kevin Y., Chirarattananon, Pakpong, Fuller, Sawyer B., & Wood, Robert J (2013). Controlled flight of a biologically inspired, insect-scale robot. *Science*, *340*(6132), 603–607.

Murray, Richard M. (2017). *A mathematical introduction to robotic manipulation*. CRC press.

Narendra, Kumpati S., & Annaswamy, Anuradha M. (2012). *Stable adaptive systems*. Courier Corporation.

Olfati-Saber, Reza (2002). Near-identity diffeomorphisms and exponential/spl epsi/-tracking and/spl epsi/-stabilization of first-order nonholonomic SE (2) vehicles. In *Proc. American control conference: Vol. 6*, (pp. 4690–4695). IEEE.

Ristroph, Leif, Ristroph, Gunnar, Morozova, Svetlana, Bergou, Attila J., Chang, Song, Guckenheimer, John, et al. (2013). Active and passive stabilization of body pitch in insect flight. *Journal of the Royal Society Interface*, *10*(85), Article 20130237.

Shen, Jinglai, Sanyal, Amit K., Chaturvedi, Nalin A., Bernstein, Dennis, & McClamroch, Harris (2004). Dynamics and control of a 3D pendulum. In *Proc. international conference on decision and control: Vol. 1*, (pp. 323–328). IEEE.

Su, Weihua, & Cesnik, Carlos (2011). Flight dynamic stability of a flapping wing micro air vehicle in hover. In *Proc. AIAA/ASME/ASCE/AHS/ASC structures, structural dynamics and materials conference* (pp. 2009).

Taha, Haithem E., Hajj, Muhammad R., & Nayfeh, Ali H. (2012). Flight dynamics and control of flapping-wing MAVs: a review. *Nonlinear Dynamics*, *70*(2), 907–939.

Taha, Haithem E., Woolsey, Craig A., & Hajj, Muhammad R. (2015). Geometric control approach to longitudinal stability of flapping flight. *Journal of Guidance, Control, and Dynamics*, *39*(2), 214–226.

Teoh, Zhi Ern, Fuller, Sawyer B., Chirarattananon, Pakpong, Pérez-Arancibia, Néstor Osvaldo, Greenberg, Jack D., & Wood, Robert J (2012). A hovering flapping-wing microrobot with altitude control and passive upright stability. In *Proc, international conference on intelligent robots and systems* (pp. 3209–3216).

Yang, Xiufeng, Chen, Ying, Chang, Longlong, Calderón, Ariel A., & Pérez-Arancibia, Néstor O. (2019). Bee+: A 95-mg four-winged insect-scale flying robot driven by twinned unimorph actuators. *IEEE Robotics and Automation Letters*, *4*(4), 4270–4277.

Zhang, J., Fei, F., Tu, Z., & Deng, X. (2017). Design optimization and system integration of robotic hummingbird. In *Proc. international conference on robotics and automation* (pp. 5422–5428). IEEE.

Zhang, J., Tu, Z., Fei, F., & Deng, X. (2017). Geometric flight control of a hovering robotic hummingbird. In *Proc. international conference on robotics and automation* (pp. 5415–5421). http://dx.doi.org/10.1109/ICRA.2017.7989638.

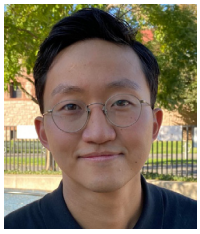

Nak-seung P. Hyun received the B.S. degree in electrical engineering in 2009 from Korea University, and the M.S. degrees in mathematics and electrical engineering in 2013, and Ph.D. degree in electrical engineering in 2018 from the Georgia Institute of Technology. He is currently a postdoc fellow at Harvard University since 2018, focusing on bio-inspired robotics control and impulsive robot control in Harvard Microrobotics Laboratory.

His recent research addresses a new framework of causal modeling of impulsive systems, optimal path planning for multi-agent system. His research interest lies in the adaptive control, contraction theory and geometric control with particular applications to bio-inspired robotic systems.

Rebecca McGill is a Ph.D. candidate in Engineering Sciences at Harvard University. She received her B.S. degree from the Massachusetts Institute of Technology in Mechanical Engineering in 2017, and her M.S. degree in Engineering Sciences from Harvard University in 2019. She is currently supported by the NSF Graduate Research Fellowship Program for her work in modeling and control of micro-aerial vehicles with the Harvard Microrobotics Laboratory.

Robert J. Wood is a Professor in the Harvard School of Engineering and Applied Sciences and a National Geographic Explorer. Wood's work focuses on the mechanical side of artificial intelligence, creating novel microrobots and soft and wearable robots. He is the winner of the DARPA Young Faculty Award, NSF Career Award, ONR Young Investigator Award, Air Force Young Investigator Award, Technology Review's TR35, the Presidential Early Career Award for Scientists and Engineers, the NSF Alan T. Waterman award, the inaugural Max Planck–Humboldt Medal, and multiple best paper awards.

Scott Kuindersma is a Research Scientist at Boston Dynamics where he leads a team of engineers focused on pushing the boundaries of autonomous, athletic, and expressive dynamic behavior on Atlas. Previously he held positions as an Assistant Professor of Engineering and Computer Science at Harvard University and a postdoc at MIT CSAIL where he led the control effort for the MIT DARPA Robotics Challenge team. He received his Ph.D. in Computer Science from the University of Massachusetts Amherst in 2012 while being supported by a NASA Graduate Fellowship. Scott's work has been recognized through several awards, including video and conference presentation awards at AAAI and RSS, faculty awards from Sony and Google, and the 2016 Best Paper of the Year award from the IEEE Technical Committee on Whole-Body Control.